Impact of atmospheric conditions and levels of urbanisation on the relationship between nocturnal surface and urban canopy heat islands

Feng, Jiali; Cai, Xiaoming; Chapman, Lee

DOI:
10.1002/qj.3619

Document Version
Peer reviewed version

Citation for published version (Harvard):
Feng, J, Cai, X & Chapman, L 2019, 'Impact of atmospheric conditions and levels of urbanisation on the relationship between nocturnal surface and urban canopy heat islands', *Quarterly Journal of the Royal Meteorological Society*, vol. 145, no. 724, pp. 3284-3299. https://doi.org/10.1002/qj.3619

Impact of atmospheric conditions and levels of urbanisation on the relationship between nocturnal surface and urban canopy heat islands

Jiali Feng,[a] Xiaoming Cai,[a*] and Lee Chapman[a]

[a] School of Geography, Earth and Environmental Sciences, University of Birmingham, Birmingham B15 2TT, UK;

*****Correspondence to: Xiaoming Cai, School of Geography, Earth and Environmental Sciences, University of Birmingham, Birmingham B15 2TT, UK
Email: x.cai@bham.ac.uk

This article has been accepted for publication and undergone full peer review but has not been through the copyediting, typesetting, pagination and proofreading process which may lead to differences between this version and the Version of Record. Please cite this article as doi: 10.1002/qj.3619

Abstract

Previous investigations of urban heat island (UHI) are primarily focused either on the canopy heat island intensity ($aUHII$) derived from weather stations, or on the surface urban heat island intensity ($sUHII$) derived from satellite instruments. Research of the relationship between $sUHII$ and $aUHII$ (the $sUHII$-$aUHII$ relationship) is limited and this study attempts to further progress this possibility by examining the night-time $sUHII$-$aUHII$ relationship for three factors: season, wind speed, and basic landuse categories modified from local climate zones (urban / suburban), in Birmingham, UK. Using high resolution datasets of canopy air temperature from Birmingham Urban Climate Laboratory and land surface temperature from the MODIS instrument aboard the Terra and Aqua satellites, with a unique methodology of regression analysis, confidence ellipse analysis of covariance (ANCOVA), and 2-D Kolmogorov-Smirnov (K-S) tests, statistical evidence is provided to present the varying patterns and magnitudes between $sUHII$ and $aUHII$. The significance of the impact of the three considered factors is clearly supported by the statistical tests. The results indicate that satellite data can be used to infer $aUHII$ with a higher confidence for low wind speed conditions. Results also demonstrate better confidence in the approach for summer and spring seasons, and for more urbanised sites. Indeed, the analysis potentially indicates that wind advection is a key factor for the investigation of the $sUHII$-$aUHII$ relationship. Overall, the methods used here are transferrable to other cities and/or can be used to guide further research to explore the $sUHII$-$aUHII$ relationship under other environmental conditions.

KEYWORDS

Surface Urban Heat Island; Canopy Heat Island; Land Surface Temperature; Temperature; Local Climate Zone; Satellite; Urban; Wind speed;

1. Introduction

The Urban Heat Island (UHI) - the phenomenon that the temperature in urban areas is warmer than the surrounding rural areas, has been investigated for several decades due to its potential impacts on human life in urban areas (Voogt and Oke, 2003). UHI has been well studied and quantified in many different cities (Kolokotroni and Giridharan, 2008, Shao et al., 2006, Streutker, 2002, Morris et al., 2001). However, it remains a compelling focus in urban climatology because the land-atmosphere interaction is far more complicated than originally hypothesised. The land-atmosphere interactions at city scale are based on various energy and moisture exchanges within a complicated urban ecosystem with feedback systems between the land-atmosphere interactions and the whole urban ecosystem that are still ambiguous, therefore there are more uncertainties in UHI studies (Jain et al., 2017).

The intensity of the canopy UHI ($aUHII$) is generally quantified from a comparison of air temperatures (T_a) derived from weather stations within the urban canopy layer (UCL) with reference sites in rural areas (Oke, 1982). In this way, the energy exchange processes controlling the characteristics of $aUHII$ are dominantly controlled by site-specific characteristics and the microscale turbulence processes. However, in the frequent absence of urban weather stations, surface heat island intensity ($sUHII$) can instead be derived using the land surface temperature (T_s) from satellite instruments (Tomlinson et al., 2011). $sUHII$ data provide opportunities to study the UHI in a spatially continuous way with higher spatial resolution and lower cost compared to the approach of urban meteorological networks (UMN: (Muller et al., 2013)). However, there exist significant compromises of low temporal resolution (i.e. a daily snapshot, and the measurement of T_s as opposed to T_a). Therefore, it is

both advantageous and practical to investigate the relationship between $sUHII$ and $aUHII$ (the $sUHII$-$aUHII$ relationship) in order to work backwards and estimate air temperatures from surface temperatures. However, this is a complex task with T_s having a different physical meaning compared to T_a. Satellites have a view of ground surface from a sensor that receives the average radiative information from the surface for each pixel which depends on the satellite viewing angle. Explicitly, only radiative source areas and surfaces within the line of sight of the sensor can be detected. In this case, the different physical representations between T_s and T_a in the complicated city-atmosphere system induce more uncertainties between $sUHII$ and $aUHII$.

As regards the relationship between the surface temperature and the air temperature somewhere above the roughness elements in the atmospheric surface layer (the T_s - T_a relationship), applicability of the Monin-Obukhov similarity theory (MOST) has been well justified (Foken, 2006). However, to apply MOST to link *urban canopy air temperatures* and *satellite products of land skin temperatures* for an urban surface is extremely difficult. This might be attributed to the insufficient accuracy of the satellite data (e.g., accuracy of 1℃ of MODIS land surface temperature product over lake or grassland areas (Wan et al., 2004) and an error of 3-5% of MODIS nighttime radiation data in Basel, which corresponds to an error of about 2.2-3.7 K for the land surface temperature (Wicki et al., 2018)) and the difficulty of converting satellite-sensed land surface temperature to aerodynamic surface temperature for estimating heat fluxes in MOST (Zibognon et al., 2002), together with doubtful applicability of the MOST in the urban canopy layer.

Previous studies focused on the T_s-T_a relationship are generally based on regression models over urban areas. For example, the night-time T_s-T_a relationship was documented with strong correlations (R^2) in linear regression models from some previous studies (Table 1): R^2 value of 0.60 was demonstrated based on the data from stations in Birmingham, UK over summer 2013 (Azevedo et al., 2016). Stronger relationships ($R^2 = 0.92$) between the T_s and the minimum T_a at night-time was found in Casablanca, Morocco, from 2011 to 2012 (Bahi et al., 2016). In reality, a linear T_s-T_a relationship is likely to be significant with high R^2 values because of large variability of regional-scale background temperature and/or seasonal signals (note: the "regional-scale" here means the scales larger than the urban area of interest). Specifically, a difference of a few degrees in temperature across seasons during a year can result in a much greater magnitude than several degrees typically for $sUHII$ or for $aUHII$. For example, Sheng et al (2017) found variations of the T_s-T_a range for a station i (T_s minus T_a, $\Delta T_{s-a}^{(i)}$) between $-1.12℃ \sim 12.92℃$ (14.04℃ differences in maximum) while the range of T_s and T_a are 30℃ and 31℃ respectively. Indeed, this large seasonal variation of temperature is the dominant signal in the T_s-T_a regression models of these previous studies. The smaller variability of $sUHII$ or $aUHII$ due to different atmospheric conditions or land surface properties would be submerged in the seasonal variability (or regional-scale background temperature variability) and the physical processes determining the $sUHII$-$aUHII$ relationship would become unclear and difficult to investigate. Hence, linear models based on T_s and T_a are not very useful to estimate $aUHII$ from T_s. In contrast, a direct investigation of the $sUHII$-$aUHII$ relationship is expected to minimise the impact of

background temperature variability and/or seasonal signals, which are cancelled out in the definition of $sUHII$ $(= T_s^{(urban)} - T_s^{(rural)})$ or $aUHII = (T_a^{(urban)} - T_a^{(rural)})$.

There are numerous factors influencing the $sUHII$-$aUHII$ relationship which can be simply divided into three classifications: meteorological/climatological conditions (e.g. solar radiation, wind conditions and season etc.), land surface properties (e.g. land and cover types, albedo, and building structures etc.), instruments' issues, e.g. satellite (e.g. overpassing time, viewing angle etc.) and weather stations (e.g. accuracy, exposure etc.) characteristics. However, it is difficult to simultaneously consider all due to interdependencies and difficulties in quantification. This study will focus on the impact of season, wind speed (WS) and basic landuse categories modified from local climate zones (urban / suburban) (Stewart, 2011) on the $sUHII$-$aUHII$ relationship during night-time. All three impacts are of great importance to the $sUHII$-$aUHII$ relationship. Seasonal patterns of the $sUHII$-$aUHII$ relationship need to be considered because of the noticeable differences of the seasonal climate conditions whereas WS condition and different LCZ (i.e. landuse) can represent the evaporation or condensation tendency, atmospheric stability conditions and the amount of the reflected or emitted radiation fluxes in the urban environment. Specifically, WS in the atmospheric boundary layer can influence the transport of moisture, heat, momentum and pollutants horizontally and vertically by advection and turbulent mixing. The LCZ system is defined to classify the urban and rural sites based on "climatopes" (Wilmers, 1990) which are closely linked to surface structures and landuse types (Stewart and Oke, 2012).

In order to investigate the nocturnal *sUHII-aUHII* relationship, a unique statistical analysis combining linear regression models with two-dimensional (2-D) distribution tests is applied in this study. The high resolution T_a data from a dense UMN (Birmingham Urban Climate Laboratory, BUCL) (Chapman et al., 2015) in Birmingham, UK, along with T_s datasets from the Moderate Resolution Imaging Spectroradiometer (MODIS) are used. In addition, the reason for considering night-time period only is two-fold. Firstly, nocturnal UHI occurs more frequently than daytime UHI (Jauregui, 1997) and UHII was found to be higher than that during daytime (Kim and Baik, 2005, Lemonsu and Masson, 2002, Montávez et al., 2000, Kłysik and Fortuniak, 1999). Secondly, nocturnal UHII is not directly affected by solar radiation and the *sUHII-aUHII* relationship becomes less complicated than the one at daytime. More importantly, better agreement between *sUHII* and *aUHII* has been found during night time by previous studies (Sun et al., 2015, Anniballe et al., 2014), providing more confidence to explore the nocturnal *sUHII-aUHII* relationship in this study.

2. Methods and data

2.1 Study area and meteorological station data

2.1.1 BUCL Network

Birmingham ($52.4862° N, 1.8904° W$) is the second largest city in the UK (approximate 278 km^2) located at the centre of the England with an estimated population of 1.1 million (Birmingham City Council, 2013). Part of BUCL included an installation of 24 automatic weather stations with sensors at 3 m AGL across the whole city (more details in Chapman et al. (2015)). These 24 Vaisala WXT520 weather stations measure seven atmospheric variables including air temperature, precipitation, wind speed and wind direction etc. with average spacing of 10 km and high quality control (Warren et al., 2016). Two additional UK Met

Office weather stations complement the network (Paradise Circus and Coleshill stations), with temperature data from Paradise Circus station being particularly useful due to its location in the middle of the central business district. The Coleshill station is located outside the city, and as per other UHI studies in Birmingham, provides the rural reference site for temperature and wind speed data. This study utilises the data from 20 BUCL weather stations located within the city limits and the two stations from UK Met Office (Figure 1), during the period 1 June 2013 to 31 August 2014. This period is chosen due to the data availability.

2.1.2 Site Classification

LCZ is an indicator for urban studies which considers the surface properties and the surrounding environment of a weather station, such as the sky view factor, aspect ratio and roughness etc. (Stewart and Oke, 2012). In particular, the structures of buildings and other roughness elements are of great importance to the modification of the longwave radiation emission and reflection from the urban surface that affects both the air temperature and surface temperature. For instance, the building height and sky-view factor are key parameters for the estimation of multi-reflected radiation inside a street canyon. The different density and orientation of roughness elements can enhance anisotropy effects which produces more uncertainties in sending or receiving the radiation information from the urban surface caused by different satellite viewing angles (Voogt and Oke, 1998). Moreover, the different materials (and age) of the roughness elements have diverse heat capacities, leading to the variant storage heat fluxes and the upward longwave radiation fluxes. The magnitude of the impact on airflow varies considerably across different roughness elements, which makes the

surface-air temperature relationship substantially more complicated in urban areas. In addition, LCZ can also indirectly reflect the humidity condition for each station.

The LCZ classification of the weather stations (Figure 1) used in this study are documented in Bassett et al. (2016). There are five LCZs assigned to the weather stations in Birmingham (LCZ1: Compact high rise, LCZ2: Compact mid-rise, LCZ5: Open mid-rise, LCZ10: Heavy industry, LCZ6: Open low rise). Only one station classified as LCZ1, LCZ10 or LCZ5; three stations are classified as LCZ2 and the remaining 15 stations belong to LCZ6. The details of surface and geometric properties of different LCZs were shown by Stewart and Oke (2012).

2.2 MODIS Land surface temperature data

2.2.1 Aqua and Terra satellites

The daily T_s products (MYD11A1 and MOD11A1) in version 5 (V005) from MODIS onboard Aqua and Terra satellites with approximate 1-km spatial resolution (926.63 m) are used in this study. The T_s dataset is developed based on the generalised split-window algorithm from the two thermal infrared bands of MODIS (bands 31: $10.78 - 11.28\ \mu m$ and 32: $11.77 - 12.27\ \mu m$) (technical details for the MODIS product can be found in Wan (2007)). The MYD11A1 and MOD11A1 are stored in a hierarchical data format (HDF) including 12 scientific datasets such as day and night time T_s, satellite overpassing time and view zenith angle etc. (Wan, 2006). The downloaded datasets from Earthdata Search (https://search.earthdata.nasa.gov/search) are re-projected from the Sinusoidal projection to British National Grid for Birmingham by using ArcGIS 10.4. The satellite zenith angle (SZA) can reach $\pm 65°$ (note a negative sign of the SZA means MODIS viewing the grid from east) (Wan, 2007), and the thermal anisotropy defined as the temperature biases caused by the

variations of SZA (Lagouarde et al., 2004) could increase the uncertainty of the temperature products from MODIS, particularly for highly urbanised areas with tall buildings. T_s in urban areas is found to be higher with respect to larger sensor ZA (closer to $\pm 65°$) because of a larger percentage of wall surfaces that are expected to have higher surface temperatures compared to roof and floor surfaces viewed by satellite for large cities (e.g. Chicago and New York: Hu et al., 2016). However, in a study in Toulouse, the thermal anisotropy effect was found to diminish rapidly following sunset, becoming negligible and almost azimuthally independent in the evening (Lagouarde et al., 2012), therefore, it is not considered in this study. In summary, there are 63 and 88 images available for Aqua and Terra satellites respectively during the study period.

Although the T_s products are pre-filtered by the cloud mask (the pixel is cloud-free if it has the grid value for T_s), Wan (2008) stated that cloud contamination still exists in the V005 products since the cloud-removing scheme is unable to remove the contaminated pixels under light and moderate cloud conditions. The contaminated pixels usually refer to the extreme low temperature at the top of clouds (Mutiibwa et al., 2015). All the data used in this study have been scrutinised to ensure that there are no extreme T_s values. Moreover, a higher quality control was implemented by only using the images with no missing value for Birmingham before converting T_s to degrees Celsius from Kelvin in ArcGIS.

2.2.2 Temporal and spatial consistence between T_s and T_a

There are two available daily night-time observations from MODIS with approximate overpass times of 01:30 (Aqua satellite, from north to south) and 22:30 (Terra satellite, from south to north) local solar time across the equator. As the travel time is about 15 minutes

between the equator and Birmingham for both satellites, approximate times overpassing Birmingham are 01:15 and 22:45 local solar time for Aqua and Terra, respectively. On the basis of the small difference between local solar time and coordinated universal time (UTC) over Birmingham, the T_a dataset in this study is calculated as the hourly average values of the T_a (01:00Z - 02:00Z for Aqua and 22:00Z - 23:00Z for Terra). In addition, this study combines the data from Aqua and Terra satellites in order to increase sample size.

It is difficult to achieve spatial consistency between point-derived T_a and pixel-averaged T_s, especially over urban areas where the terrain is complex (Oke, 1988). In-situ sensed T_a is strongly associated with the turbulent source area, whereas remote-sensing T_s is determined by the radiation source areas (Oke et al., 2017). The turbulent source area of T_a cannot be defined confidently using a traditional approach (e.g. a footprint model (Kent et al., 2017)) because the measurement height (3 m AGL in this study) is within the urban canopy layer. Although the turbulence source area can be local, the selection of the sites considered their representativeness (as best as can be achieved in the heterogenous urban area) of microclimatic environments of the area on a neighbourhood scale ($\lesssim$ 1 km), which is about the spatial resolution of the satellite data of T_s. Some previous studies have investigated the spatial variability of T_a by comparing the correlations between T_a and T_s estimated from different "window sizes". However, the most appropriate spatial scales of T_a varied in different study areas. For example, 200 m, 450 m and 700 m were found to be the most appropriate spatial scale of T_a for urban, suburban and rural areas respectively, in Hong Kong, China (Nichol and Wong, 2008). Although the spatial variability is not the key aim in this

study, a simple correction based upon Inverse Distance Weighting (IDW) is applied to achieve the spatial consistency between T_s and T_a.

2.3 Estimation of $UHII$

In this study, $UHII$ is defined as the difference between the temperature from a weather station/pixel located in urban area ($T_a^{(i)}$ or $T_s^{(i)}$) and the temperature from a rural station/pixel ($T_a^{(r)}$ or $T_s^{(r)}$):

$$sUHII = \Delta T_s^{(i)} = T_s^{(i)} - T_s^{(r)} \quad (1)$$

$$aUHII = \Delta T_a^{(i)} = T_a^{(i)} - T_a^{(r)} \quad (2)$$

Here, i represents weather station index in urban areas (20 BUCL and 1 Met office weather stations) and r is for the rural station in the study area (Coleshill station).

2.4 Statistical methodology

Data from all stations are grouped by (1) seasons, (2) WS and (3) levels of urbanisation (urban / suburban) respectively (Table 2 provides the summary of the sample size in terms of these three variables). The influences of season, WS and levels of urbanisation on the $sUHII$-$aUHII$ relationship are initially investigated, based on linear regression models (LRM) (Montgomery et al., 2012). LRM is chosen because of its simplicity compared to other non-linear regression models and it is easier to interpret the relationship between the two variables. Significance tests for the LRM and regression coefficients (slope and intercept) are conducted subsequently based on 0.01 level of significance.

An interaction effect can exist in LRM when the impact of an independent variable on a dependent variable is affected by a third moderator variable (Jaccard and Turrisi, 2003). In

this study, the influence of the three moderator variables and the overall interaction effect is then examined by the analysis of covariance (ANCOVA) that can be used to compare two regression lines corresponding to two values of moderator variable and to show if the two regression lines (represented by their respective slope and intercept) are significantly different. For instance, LRMs are derived for four seasons, and the slopes/intercepts assessed via ANCOVA. The differences between LRMs in four seasons will be reflected by the assessment of slopes/intercepts in ANCOVA. The overall interaction effect indicates the seasonal impacts on the linear $sUHII$-$aUHII$ relationship.

Uniquely, 2-D distribution analysis using confidence ellipses is implemented in this study. These are generated at the 90% confidence level (Monette, 1990) and used to visualise the 2-D distributions connected with linear models. This step adds a useful summary of the relationship between two variables such as the means and standard deviations etc. (Friendly et al., 2013). Specifically, the x-y coordinates of the centre of the confidence ellipse are the means of the two variables, i.e. $sUHII$ and $aUHII$. The magnitude and the orientation of the ellipse are the eigenvalues and eigenvectors, respectively, of the covariance matrix for the two variables, with consideration of a given confidence level (e.g. 90% in this study). In other words, the major and minor axes of the ellipse represent the direction and magnitude of the largest and second largest spread of the data. The confidence level is chosen based on the Chi-Square distribution (Wilson and Hilferty, 1931) with specific "degrees of freedom" (representing the number of unknowns) (Spruyt, 2014). The 2-D Kolmogorov-Smirnov (K-S) test is then applied to further investigate the goodness-of-fit for the 2-D distributions of the $sUHII$-$aUHII$ relationship in terms of season, WS and LCZ. The 2-D K-S test developed by

Peacock (1983) is the analogue of the one-dimensional K-S test. The statistical result of the 2-D K-S test is the maximum difference of the corresponding integrated probabilities (the fraction of the points for a quadrant) in four natural quadrants at a given point in the data, called statistic D, which is the maximum absolute difference between the two cumulative distributions. The key parameters calculated in the K-S test are demonstrated in the study of Peacock (1983).

3. Results

LRMs are generated based on different moderator variables, where a is slope and b is intercept coefficient, and the independent (x) and dependent (y) variables are $sUHII$ and $aUHII$ respectively:

$$y = a * x + b \quad (3)$$

The LRM for whole datasets was also calculated to compare with the LRMs with consideration of any moderator variable:

$$y = 0.57x + 0.26, \ (R^2 = 0.35) \quad (4)$$

This study is primarily focused on the regression output (R^2, slope and intercept) from the LRMs, the confidence ellipses and the results from ANCOVA and K-S tests based on the three moderator variables. The R^2 value herein is interpreted as the percentage of the variation of $aUHII$ explained by the regression equation using $sUHII$ as the only independent variable. The slope coefficient effectively represents an increment of the $aUHII$ for every one degree increment of the $sUHII$, which can reflect the physical processes between surface and air. The intercept coefficient represents the value of $aUHII$ when the

$sUHII$ becomes zero. A positive value of the intercept indicates that the $aUHII$ still exists despite the lack of a $sUHII$. Although there is limited available physical information from the interpretation of the intercept, the value of the intercept does appear to be statistically correlated with the slope.

3.1 The effect of wind speed

$sUHII$ and $aUHII$ data from all stations are grouped as low (WG1: WS<2m/s), median (WG2: WS=2-4m/s) and high (WG3: WS=4-6m/s) WS conditions. The linear regressions and 2-D distributions between $sUHII$ and $aUHII$ are visualised in Figure 2A and 2B. The mean values of the $sUHII$ and $aUHII$ decrease with increasing WS, illustrated by the moving tendency of the centre of the estimated ellipses to (0,0). The ratio of major axis to minor axis is largest in the WG2, indicating the more apparent linear relationship.

The slope coefficient of the regression models becomes smaller with increasing WS (Figure 2A), which suggests the reduced sensitivity of the $aUHII$ compared to $sUHII$. In addition, the intercept coefficients tend to decrease with increasing WS as well, demonstrating the smaller $aUHII$ when $sUHII$ comes to zero under high WS condition. It should be noticed that most values of intercept are positive due to the prevalent existence of the UHI phenomenon in cities.

The R^2 value of the regression model is highest in median WS group (WG2) ($R^2 = 0.35$) but is slightly lower in WG1 ($R^2 = 0.27$). In WG3, both $sUHII$ and $aUHII$ are small so that the influence from other processes become visible and these are viewed as noise in Figure 3 where the R^2 value is smallest (0.09). The decrease of R^2 values from WG2 to WG3 suggests

a smaller sensitivity of $sUHII$ to $aUHII$. Moreover, the decrease of the slopes under high WS condition is also indicative to the decline of the R^2 values. For example, a slope value of zero implies that the value of $aUHII$ will be independent of $sUHII$. Thus, it is much less confident to estimate $aUHII$ based on $sUHII$ under high WS condition. In addition, the R^2 values decreased after classifying the data based on different WS because the data are subtracted to a more specific or smaller range.

The results from ANCOVA (Table 3) for the three wind groups (WGs) show that the overall WS effect on the linear $sUHII$-$aUHII$ relationship is significant at 99% confidence level (F=9.77). Moreover, the slopes and intercepts in the three WS groups are all significantly different at the 99% confidence level. The K-S test (Table 4) illustrates that the 2-D distributions are significantly different at 0.001 level in the three WGs. According to the D statistics, a 76% difference of the 2-D $sUHII$-$aUHII$ distribution is found between WG1 and WG3, followed by 46% between WG2 and WG3 and 39% between WG1 and WG2.

3.2 Seasonal differences

The LRM and confidence ellipses for the $sUHII$-$aUHII$ relationship for four seasons are shown in Figure 3A and 3B. It is evident that the centre points of the ellipses, representing the mean values of $sUHII$ and $aUHII$, have a clear tendency to move towards the origin (0,0) in the order of summer, spring, autumn and winter, indicating a greater magnitude of the UHI in summer and spring. The longer major axis of the confidence ellipses and the larger ratio of major axis to minor axis are also indicative of the stronger linear trend in summer and spring. Although the available data in winter (n=257) is more limited than other seasons (Table 2),

the lowest ratio of major axis to minor axis and the more rounded shape of the confidence ellipses indicate that the $sUHII$-$aUHII$ relationship is much less prominent in winter.

Figure 3A also shows the summary of the estimated linear regression model in four seasons. The rate of change of the linear models (slope) is small for autumn and winter. All LRMs were statistically significant at 99.9% confidence level except for the intercept in winter (not shown here), suggesting less reliability of the linear models in colder weather. In Figure 3A, the low R^2 values for autumn and winter suggest more uncertain influencing factors affecting the $sUHII$-$aUHII$ relationship. A more limited sample size (Table 2) in autumn and winter due to fewer clear-sky nights is also one of the potential factors causing the lower R^2 values. Moreover, the smaller magnitude of both $sUHII$ and $aUHII$ in colder seasons contributes to the reduced confidence of the estimated LRM. Furthermore, stronger anthropogenic heat (especially from space heating) may be responsible for the less correlated data between $sUHII$ and $aUHII$, leading to the decrease of R^2 values as well.

Table 5 and Table 6 demonstrate the results from the subsequent ANCOVA and K-S test that present interaction effects and differences of intercepts and slopes between different seasons and the significant test of 2-D distributions between $sUHII$ and $aUHII$, respectively. Overall, results from the two statistical tests provide the confidence to support the previous discussion of the regression models. The seasonal impacts (overall effect) are significant at 0.001 level in the group of four but less significant in these two groups – "spring and summer" and "autumn and winter". However, K-S test (Table 5) demonstrates that in all tests, $D > D_{\alpha(\alpha=0.001)}$ where $D_{\alpha(\alpha=0.001)}$ is the critical value of the statistics D at 99.9% confidence

level; in other words, the 2-D distributions between $sUHII$ and $aUHII$ are all significantly different at 99.9% confidence level between any pair of two seasons from the K-S test result. Moreover, the D statistics represent the maximum 2-D distribution differences as well as the overlapping portions in a quadrant of the data points in a paired group. In particular, the differences are greater in "summer, autumn (45%)" and "summer, winter (55%)" paired groups. In addition, the differences between D and D_a ($\Delta D = D - D_a$) are greatest in "summer, autumn" and "summer, winter" paired groups, which also indicated the bigger differences of the distribution comparing summer to autumn and winter.

3.3 The role of site characteristics

The analysis is conducted to infer the role of LCZ. Due to the limited stations for some LCZs in the city, LCZ1 and LCZ2 are classified as urban group, whereas LCZ5, LCZ6 and LCZ10 are classified as suburban group. Figure 4 shows the confidence ellipses and linear regression models based on the urban and suburban groups. As expected, the $UHII$ is stronger for urban group and weaker for suburban group whose ellipse's centre is closer to (0,0). The longer major axis and the larger ratio of the major to the minor axis indicate a more noticeable linear relationship for urban group.

Overall, differences in the regression coefficients between urban and suburban groups are evident, which increase from urban to suburban group for both slope and intercept. The pattern of the slopes of the LRMs indicates a lower sensitivity of the $aUHII$ than $sUHII$ for suburban group. In terms of intercepts, the positive values in both urban and suburban linear regression models indicate that $aUHII$ tends to exist even when the $sUHII$ becomes zero.

Meanwhile, the higher value of the intercept suggests that the magnitude of the $aUHII$ tends to be higher in urban than suburban group.

R^2 values are higher in urban group (0.46) than suburban group (0.28). Compared with the R^2 value of 0.35 for the whole dataset, a higher R^2 value of 0.46 is obtained for the subset, urban group. It is therefore concluded that among the three moderator variables (season, wind speed, and LCZ), LCZ can increase the R^2 value of the linear $sUHII$-$aUHII$ relationship for a subset of data. This is consistent with the finding in Figure 4B that for the subset of 'urban', both the major axis length and ratio of major to minor axis are the largest among all subsets for all three moderator variables (see Figures 2B & 3B).

The ANCOVA (Table 7) and K-S tests (Table 8) are conducted for each LCZ subset and for the urban and suburban subsets. With respect to different LCZs, the two statistical tests show more evidence for the comparison between different paired groups. The results from ANCOVA test (Table 7) illustrate that the differences between the regression models are mostly significant among many of the different paired groups for LCZs (green highlighted section). However, the differences of some paired groups: LCZ6 and LCZ1, LCZ6 and LCZ2 are not significant. Moreover, additional statistical tests for slope and intercept (blue highlight section) infer that the LRM differences between some paired groups of LCZs are not significant in this respect. From the K-S test (Table 8), the 2-D distributions are all significantly different between the five LCZs ($p < 0.001$). Moreover, it is evident that the differences between the values of D and D_a (ΔD) become larger when the compared group is less urbanised for each column. For example, the values of ΔD increase as the following

order of the paired groups: “LCZ1, LCZ2”, “LCZ1, LCZ5”, “LCZ1, LCZ10”, “LCZ1, LCZ6”. In contrast, the ΔD values will decrease when the paired groups are more similar, such as “LCZ10, LCZ6”.

For the urban and suburban groups, ANCOVA test (Table 7) provides sufficiently high confidence levels for the differences of the linear $sUHII$-$aUHII$ relationship. Moreover, the highest F value (F=11.20) is found in the urban and suburban paired group, which indicates the reliability of this classification compared to analyse individual LCZ. The K-S test (Table 8) shows that the D statistics ($D = 0.32$, $D_a = 0.10$) are almost the largest among all other paired groups at 0.01 confidence level, which also indicates the urban and suburban classification is appropriate and can be implemented for further analysis.

4. Discussion

The statistical significance of the two regression coefficients (slope and intercept) of the LRMs analysed in Sections 3.1-3.3 can indicate some useful information about the relationship between $sUHII$ and $aUHII$. In fact, the slope can be related to the covariance between $sUHII$ and $aUHII$ (denoted by $Cov(sUHII, aUHII)$) and the standard deviation of these two variables (denoted by SD_{sUHII} and SD_{aUHII}) (Fisher, 1992):

$$slope = \frac{Cov(sUHII,aUHII)}{Var(sUHII)} = r \cdot \frac{SD(aUHII)}{SD(sUHII)} \quad (5a)$$

$$r = \frac{Cov(sUHII,aUHII)}{SD(sUHII)\cdot SD(aUHII)} \quad (5b)$$

where r is the correlation coefficient ($r = \sqrt{R^2}$) and $Var(sUHII)$ is the variance of $sUHII$. Table 9 lists the results of the statistical parameters for $sUHII$ and $aUHII$. The following discussion will be based on these statistical quantities.

4.1 Difference of the $sUHII$-$aUHII$ relationship under three WGs

According to the derived LRMs and confidence ellipses in Section 3.1, an increase of WS reduces the slope and intercept values. This is consistent with the rotation of the confidence ellipses with WS. From Table 9, the decrease of both SD_{aUHII} and SD_{sUHII} with increasing WS indicates that WS can reduce the variabilities of both $aUHII$ and $sUHII$ by turbulent mixing, but is more effective for $aUHII$, which is reduced to 0.45℃ for WG3, compared with 0.81℃ for $sUHII$. These imply that T_a is more affected by WS than T_s due to different processes influencing these two variables by wind flow. In addition, $Cov(sUHII, aUHII)$ decreases significantly with WS, indicating a much weaker joint variability of $sUHII$ and $aUHII$ for WG3. This suggests that there are more similarities between $sUHII$ and $aUHII$ for low WS scenarios, but more dissimilarities for high WS scenarios. The implication is that use of satellite data to infer $aUHII$ has a higher confidence for low WS conditions than for high WS conditions.

The slope is likely to be related to wind advection. The spatial pattern of $aUHII$ is shifted by advection due to the wind transport of air temperature directly (Bassett et al., 2016, Heaviside et al., 2015). In contrast, the spatial pattern of $sUHII$ should be more influenced by the local-scale radiation processes and less affected by advection (the surface heat needs to be

transferred to air first before the advection and heat transfer back to the surface in a downwind location). The shift of spatial pattern between $sUHII$ and $aUHII$ can be reflected by the statistical value of $Cov(sUHII, aUHII)$ which decreases with WS. In other words, the covariance between $sUHII$ and $aUHII$ is increasingly smaller under higher WS conditions. From Equation (5a), the value of the slope of LRM equates to the ratio of $Cov(sUHII, aUHII)$ to $Var(sUHII)$, and it can also be interpreted as a normalised covariance. As seen in Table 9, although $Var(sUHII)$ decreases with WS (by about 50% from WG1 to WG3, estimated from the values of SD_{sUHII}), the decrease of $Cov(sUHII, aUHII)$ with WS is much faster (~83% from WG1 to WG3). Therefore, the decrease of slope with increasing WS is due to the change of the $Cov(sUHII, aUHII)$ from statistical aspect. Moreover, a higher WS tends to destroy the nocturnal stable layer over the rural surface and to entrain the warmer air aloft downwards to warm the T_a there, thus reducing the magnitude of $aUHII$. Although this process may also warm the T_s at the rural site, the magnitude of reduced $sUHII$ could be smaller. Such reductions of UHII can be reflected from the magnitudes of SD_{sUHII} and SD_{aUHII} in Table 9. Consequently, the slope of the LRM will be reduced because the slope is linearly proportional to the SD ratio (Equation 5a).

In Figure 2B or 2C, the centres of the ellipses represent the mean values of $UHII$: ($\overline{sUHII}$, $\overline{aUHII}$). The results show that all three centres are below the 1:1 long-dashed line. This is interpreted as a higher $\overline{sUHII}$ than $\overline{aUHII}$ for all wind groups, consistent with the dominating processes of storage-heat release and radiative trapping in urban areas. For the low WS group, WG1, the circle is very close to the 1:1 long-dashed line, indicating that $\overline{sUHII} \approx \overline{aUHII}$.

From the perspective of processes, under calm conditions, surface temperature drops rapidly by emitting longwave radiation, cooling the air near the ground, and the surface layer may become extremely stable and shallow (T_s is lower than T_a). Therefore, a thermal inversion may be formed near the surface with a limited amount of heat in the shallow surface layer being transferred to the ground, reducing $T_a^{(r)}$ more compared with windier conditions under which the surface layer is deeper. This leads to similar magnitudes of $T_a^{(r)}$ and $T_s^{(r)}$ within the shallow surface layer and therefore, the characteristics of $aUHII$ and $sUHII$ are similar because the magnitude of UHII is sensitive to the extent of rural radiative cooling. For a high WS group, WG3, Figure 2C shows that $\overline{aUHII}$ is close to zero, whereas $\overline{sUHII}$ still has a finite value. As discussed above, surface loses radiative energy irrespective of high WS but the nocturnal stable layer (or temperature inversion) above the surface layer over the rural site could be destroyed under high wind speed conditions, leading to an entrainment of warmer air in the residual layer aloft into the surface layer (Stull, 1988) and a subsequent less cooling effect of air temperature in rural areas. Therefore, $\overline{aUHII}$ may reach zero while $\overline{sUHII}$ still exists.

4.2 Effect of climatology (seasonal effect)

Figure 3 indicates that both $sUHII$ and $aUHII$ are stronger in summer and spring, and weaker in winter and autumn at night-time. These were also reported by many previous studies (Fenner et al., 2014, Van Hove et al., 2015, Peng et al., 2011, Meng and Liu, 2013). Studies carried out in central Europe argued that the development of the UHI is favourable during summer at night-time because of the greater likelihood of clear skies and lighter winds for

mid-latitudes climate (Fortuniak et al., 2006, Kłysik and Fortuniak, 1999). Furthermore, the seasonal variation of rural thermal admittance related to soil moisture is considered as another significant contributor to seasonal differences of UHI (Arnfield, 1990, Runnalls and Oke, 2000). The seasonality of soil moisture has been found to be related to the heat island intensity in London (Zhou et al., 2016). Likewise, the drier seasonal climate during summer in Birmingham may reduce soil moisture, and therefore thermal admittance differences between urban and rural areas become greater (Oke et al., 1991, Imamura, 1991). The increased thermal admittance differences cause larger differences of the cooling rates between urban and rural areas, which could contribute to faster decrease of temperature at rural site and increase of UHI consequently during the summer period (Runnalls and Oke, 2000). Moreover, the increase of solar insolation during summer time induces a greater amount of energy to be stored and released during daytime and night time respectively. Fenner et al. (2014) stated that the decoupling of the urban sites from the rural site is largely strengthened due to the stronger radiative forcing during summer compared to winter, leading to the strongest UHI developed on summer nights. In addition, the timing of sunset is between 21:00Z and 22:00Z during the summer period, which is close to the satellite passing time mentioned in Section 2.2.2. This means that cooling might start later compared to other seasons, which could induce a larger UHII, especially $sUHII$ (e.g., larger mean differences of $sUHII$ compared to $aUHII$ (represented by the horizontal and vertical distance of the centre points of ellipses respectively) between summer and spring). However, causative factors governing the seasonal differences of the magnitude of both $sUHII$ and $aUHII$ are still

needed to be further explored, e.g., seasonal variations of rural moisture and heat storage or temperature cooling rates differences between urban and rural areas etc.

Table 9 shows very high values of $Cov(sUHII, aUHII)$ for summer (0.85) and spring (0.61) and a very low value for winter (0.16), whereas the magnitudes of SD_{sUHII} and SD_{aUHII} show much less contrast across the seasons. This is consistent with the slope values in Figure 3A, larger slopes for spring and summer, and smaller for autumn and winter. The values of $Cov(sUHII, aUHII)$ and the slopes suggest some similarities between $sUHII$ and $aUHII$ for summer, but dissimilarities for winter. The implication is that use of satellite data to infer $aUHII$ has a higher confidence for summer and spring than for autumn and winter. The result is also in line the R^2 values shown in Figure 3A.

To link the results here to mechanisms in the WS categorisation, we have calculated the mean wind speed for the four seasons: Spring: 1.98 m/s, Summer: 1.95 m/s, Autumn: 2.21 m/s, Winter: 3.18 m/s. Use of the results in 3.1 and discussions in 4.1 suggests that low wind speed for spring and summer is one of the reasons why the magnitudes of both $sUHII$ and $aUHII$ and the slopes of the LRMs are greatest among four seasons. The values of ($\overline{sUHII}$, $\overline{aUHII}$) represented by the centres of the ellipses in Figure 3C can be partially explained by the WS mechanism discussed earlier, i.e. the faster WS is, the smaller the values of $\overline{sUHII}$ and $\overline{aUHII}$. As the values of mean wind speed are similar for summer and spring, the larger $\overline{sUHII}$ and $\overline{aUHII}$ for summer is explained by stronger solar insolation. Although the mean wind speed for winter is much larger than that for autumn, the values of $\overline{sUHII}$ and $\overline{aUHII}$ for winter are as large as those for autumn. This could be attributed to the release of

anthropogenic heat due to more energy consumption during the winter season. In addition, the reduced surface albedo because of the removal of crops in rural areas and the loss of canopy cover in urban areas could increase the absorption of solar radiation during winter, which could be one of the reasons for similar magnitude of $\overline{sUHII}$ and $\overline{aUHII}$ between autumn and winter seasons.

4.3 Difference of the $sUHII$-$aUHII$ relationship from urban to suburban group

The results for two land-use groups are shown in Figure 4. It is worth mentioning that except for data missing scenarios, both groups of data cover similar wind conditions and seasonal distributions. Therefore the differences shown in Figure 4 should be mainly attributed to the disparity of the land-cover characteristics between the two groups. It is evident in Figure 4C that larger $\overline{sUHII}$ and $\overline{aUHII}$ are found for the Urban group than for the Suburban group. In addition, a larger slope is also evident for the urban group, which is caused by the larger joint variability between $sUHII$ and $aUHII$, i.e. $Cov(sUHII, aUHII)$, for the urban group, as shown in Table 9. In order to gain more insight into the relationships, a quadrant analysis is conducted and the results are shown in Figure 5, in which the values of $(\overline{sUHII}, \overline{aUHII})$ represented by the circle of the ellipse are used to separate the parameter space into four quadrants, Z1-Z4. A higher percentage of data points in Z1 (in which $sUHII > \overline{sUHII}$ AND $aUHII > \overline{aUHII}$) and Z3 (in which $sUHII < \overline{sUHII}$ AND $aUHII < \overline{aUHII}$) will enhance the value of $Cov(sUHII, aUHII)$, and increase the slope of the LRM. Likewise, a higher percentage of data points in Z2 (in which $sUHII < \overline{sUHII}$ AND $aUHII > \overline{aUHII}$) and Z4 (in which $sUHII > \overline{sUHII}$ AND $aUHII < \overline{aUHII}$) will reduce the value of $Cov(sUHII, aUHII)$,

decreasing the slope of the LRM. One imperative factor that may have an impact on the distribution of data points is wind advection. Warm advection can raise T_a promptly with T_s unchanged or warmed later; this could induce a greater chance of the Z2 scenario. Similarly, cold advection could induce a greater chance of the Z4 scenario. It should be noticed that an urban site near the city centre has a small chance of experiencing warm advection but is more subject to cold advection; this is supported by the data in Figure 5A, showing 7% of Z2 and 12% of Z4. The stations in the suburban group in Birmingham, however, are scattered around the city centre, some near rural area and some close to parks (Figure 1). Therefore, they are collectively subject to both warm advection (from upwind urban patches) and cold advection (from upwind rural area or nearby parks), consequently yielding a higher percentage for Z2 (14%) and for Z4 (13%) as shown in Figure 5B. Accordingly, these explain that the value of $Cov(sUHII, aUHII)$ is higher for the urban group (1.04 in Table 9) and lower for the suburban group (0.60 in Table 9). Considering that SD_{sUHII} is similar for the two groups (1.23 and 1.12 in Table 9), according to Equation 5a, the slope of LRM is higher for the urban group than the suburban group; the result is also shown in Figure 4A. Based on the discussions, we may conclude that the data of $sUHII$ for the urban sites are better correlated with $aUHII$ compared with those of the suburban sites. The implication is that wind advection (together with other factors not discussed here) may obscure the interpretation of satellite-sensed land surface temperature for the purpose of representing $aUHII$ by $sUHII$, and caution should be taken particularly for suburban locations.

In addition, the positive intercept values in the regression models might provide an implication of the "lagged development" of $aUHII$ compared to $sUHII$ which is also

indicated by Oke et al. (2017). This implication is based on the assumption that the temporal variation of $sUHII$ and $aUHII$ is similar in pattern but with a time lag during night time due to the processes of heat storage in the surface during the daytime and heat transfer from the surface to the air during the night. According to Oke (2002), the typical temporal variation of $aUHII$ is that $aUHII$ will increase after sunset and reach the maximum a few hours after sunset and it tends to decrease afterwards. The "lagged development" of $aUHII$ means that the increase and decrease of $sUHII$ take place earlier compared to $aUHII$ during night time. Therefore, the point where $sUHII$ approaches 0 but $aUHII > sUHII \sim 0$ (intercept value) will appear at some time during the development of UHI. For a stronger UHI event, this point may occur later at night, whereas for a weak UHI event, this point may occur earlier (e.g. at the hours of this analysis). The positive intercept values are consistent based on different seasons and WS classification. In addition, the intercept value tends to be 0 when the wind speed increases (Figure 2A), indicating that the lag effect diminishes with increasing WS. However, most of the data points are away from the (0,0) point and we don't have strong supporting evidence from our data.

5. Conclusions

An investigation of the $sUHII$-$aUHII$ relationship has been challenged by the complicated interactions between varying meteorological processes and the multi-scale, heterogeneous urban environment. However, using the methodology outlined in this paper, the linear $sUHII$-$aUHII$ relationship is shown to be statistically reliable, and clearer characteristics of this relationship are revealed for the categorised data groups based on three moderator

variables: wind speed (WS), season and level of urbanisation. The following results are highlighted: (1) The linear $sUHII$-$aUHII$ relationship significantly varies with respect to the three moderator variables; results indicate that satellite data can be used to infer $aUHII$ with a higher confidence for low wind speed conditions. Results also demonstrate better confidence in the approach for summer and spring seasons and for more urbanised sites. (2) For the WS category, the decrease of the slope of LRM with increasing WS is explained by the same decreasing trend of the value of covariance between $sUHII$ and $aUHII$, $Cov(sUHII, aUHII)$; subsequently, the decreasing $Cov(sUHII, aUHII)$ with WS is partially attributed to wind advection which causes different shifts of the spatial pattern of $sUHII$ and $aUHII$. (3) The larger slopes in summer and spring are partly explained by the lower WS conditions during these two seasons; however, further investigations of other causative factors are needed. (4) The quadrant analysis applied to two land-use groups (urban vs. suburban) yields the evidence to support the argument that wind advection may be responsible for the lower correlation between $sUHII$ and $aUHII$ for the suburban group. Therefore different impacts of wind advection on T_a and T_s may affect the representation of $aUHII$ by $sUHII$, and cautions should be taken particularly for suburban locations.

In summary, investigation into the $sUHII$-$aUHII$ relationship based on LRMs has previously been found difficult by a few studies. Compared with previous studies, the unique combination of analyses adopted in this study to investigate the $sUHII$-$aUHII$ relationship is able to provide more statistical evidence to estimate the magnitude and the range of the $aUHII$ from $sUHII$ under different conditions. In addition, the exploration of the

sUHII-aUHII relationship in this study provides more evidence and knowledge for the modelling of the T_s-T_a relationship, which may also be useful to further understand the applicability of MOST in the urban environment.

Several limitations should be highlighted in this study. Firstly, it is unfortunate that the study did not determine the same or similar sample size for each group of the data based on different stratification levels. The different sample size of the data might produce some uncertainties in the estimation of LRMs, although the statistical tests for LRMs and regression coefficients have been conducted based on the 0.01 significance level. Secondly, the generalisability of these models is subject to certain limitations. For instance, the values of regression coefficients are valid only based on these specific datasets in Birmingham, under the specific regional climate conditions during the study period. Another weakness of this study is the lack of consideration of how these three moderator variables affect the *sUHII* and *aUHII* jointly due to the limited data size.

Despite the above limitations, the study adds to the understanding of the *sUHII-aUHII* relationship. Further research based on this method needs to be conducted in other cities. Moreover, when sufficient data are available, multiple factors can be considered at the same time to study the *sUHII-aUHII* relationship and it is expected that such refined studies may yield improved outcome. In addition, *sUHII* mainly depends on the quality of the satellite datasets. It is necessary to use other or higher-resolution remote sensing data to check or to validate the results of this study in the future.

Conflict of Interests

The authors declare that there is no conflict of interests regarding the publication of this paper.

Acknowledgments

This research was supported through Automatic Weather Station data from the Birmingham Urban Climate Laboratory and Met Office Station data from the British Atmospheric Data Centre. We thank the helpful comments from the anonymous reviewers that were valuable for improving the article.

Reference

Anniballe, R., Bonafoni, S. & Pichierri, M. 2014. Spatial and temporal trends of the surface and air heat island over Milan using MODIS data. *Remote Sensing of Environment,* 150**,** 163-171.

Arnfield, A. J. 1990. Canyon geometry, the urban fabric and nocturnal cooling: a simulation approach. *Physical Geography,* 11**,** 220-239.

Azevedo, J. A., Chapman, L. & Muller, C. L. 2016. Quantifying the daytime and night-time urban heat island in Birmingham, UK: A comparison of satellite derived land surface temperature and high resolution air temperature observations. *Remote Sensing,* 8**,** 153.

Bahi, H., Rhinane, H. & Bensalmia, A. 2016. Contribution of MODIS satellite image to estimate the daily air temperature in the Casablanca City, Morocco. *International Archives of the Photogrammetry, Remote Sensing & Spatial Information Sciences,* 42.

Bassett, R., Cai, X., Chapman, L., Heaviside, C., Thornes, J. E., Muller, C. L., Young, D. T. & Warren, E. L. 2016. Observations of urban heat island advection from a high‐density monitoring network. *Quarterly Journal of the Royal Meteorological Society,* 142**,** 2434-2441.

Birmingham City Council. 2013. *2011 Birmingham Population & Migration Topic report* [Online]. Available: https://www.birmingham.gov.uk/downloads/file/9742/2011_birmingham_population_and_migration_topic_report [Accessed].

Chapman, L., Muller, C. L., Young, D. T., Warren, E. L., Grimmond, C. S. B., Cai, X.-M. & Ferranti, E. J. 2015. The Birmingham urban climate laboratory: an open meteorological test bed and challenges of the smart city. *Bulletin of the American Meteorological Society,* 96**,** 1545-1560.

Fenner, D., Meier, F., Scherer, D. & Polze, A. 2014. Spatial and temporal air temperature variability in Berlin, Germany, during the years 2001–2010. *Urban Climate,* 10**,** 308-331.

Fisher, R. A. 1992. Statistical methods for research workers. *Breakthroughs in statistics.* Springer.

Foken, T. 2006. 50 years of the Monin–Obukhov similarity theory. *Boundary-Layer Meteorology,* 119**,** 431-447.

Fortuniak, K., Kłysik, K. & Wibig, J. 2006. Urban–rural contrasts of meteorological parameters in Łódź. *Theoretical and applied climatology,* 84**,** 91-101.

Friendly, M., Monette, G. & Fox, J. 2013. Elliptical insights: understanding statistical methods through elliptical geometry. *Statistical Science,* 28**,** 1-39.

Heaviside, C., Cai, X. M. & Vardoulakis, S. 2015. The effects of horizontal advection on the urban heat island in Birmingham and the West Midlands, United Kingdom during a heatwave. *Quarterly Journal of the Royal Meteorological Society,* 141**,** 1429-1441.

Hu, L., Monaghan, A., Voogt, J. A. & Barlage, M. 2016. A first satellite-based observational assessment of urban thermal anisotropy. *Remote sensing of environment,* 181**,** 111-121.

Imamura, I. 1991. *Observational studies of urban heat island characteristics in different climate zones.* Ph. D. Thesis.

Jaccard, J. & Turrisi, R. 2003. *Interaction effects in multiple regression*, Sage.

Jain, M., Dimri, A. & Niyogi, D. 2017. Land-Air Interactions over Urban-Rural Transects Using Satellite Observations: Analysis over Delhi, India from 1991–2016. *Remote Sensing,* 9**,** 1283.

Jauregui, E. 1997. Heat island development in Mexico City. *Atmospheric Environment,* 31**,** 3821-3831.

Kent, C. W., Grimmond, S., Barlow, J., Gatey, D., Kotthaus, S., Lindberg, F. & Halios, C. H. 2017. Evaluation of urban local-scale aerodynamic parameters: implications for the vertical profile of wind speed and for source areas. *Boundary-Layer Meteorology,* 164**,** 183-213.

Kim, Y.-H. & Baik, J.-J. 2005. Spatial and temporal structure of the urban heat island in Seoul. *Journal of Applied Meteorology,* 44**,** 591-605.

Kłysik, K. & Fortuniak, K. 1999. Temporal and spatial characteristics of the urban heat island of Łódź, Poland. *Atmospheric environment,* 33**,** 3885-3895.

Kolokotroni, M. & Giridharan, R. 2008. Urban heat island intensity in London: An investigation of the impact of physical characteristics on changes in outdoor air temperature during summer. *Solar energy,* 82**,** 986-998.

Lagouarde, J.-P., Hénon, A., Irvine, M., Voogt, J., Pigeon, G., Moreau, P., Masson, V. & Mestayer, P. 2012. Experimental characterization and modelling of the nighttime directional anisotropy of thermal infrared measurements over an urban area: Case study of Toulouse (France). *Remote Sensing of Environment,* 117**,** 19-33.

Lagouarde, J.-P., Moreau, P., Irvine, M., Bonnefond, J.-M., Voogt, J. A. & Solliec, F. 2004. Airborne experimental measurements of the angular variations in surface temperature over urban areas: case study of Marseille (France). *Remote Sensing of Environment,* 93**,** 443-462.

Lemonsu, A. & Masson, V. 2002. Simulation of a summer urban breeze over Paris. *Boundary-Layer Meteorology,* 104**,** 463-490.

Meng, F. & Liu, M. 2013. Remote-sensing image-based analysis of the patterns of urban heat islands in rapidly urbanizing Jinan, China. *International journal of remote sensing,* 34**,** 8838-8853.

Monette, G. 1990. Geometry of multiple regression and interactive 3-D graphics. *Modern methods of data analysis***,** 209-256.

Montávez, J. P., Rodríguez, A. & Jiménez, J. I. 2000. A study of the urban heat island of Granada. *International journal of climatology,* 20**,** 899-911.

Montgomery, D. C., Peck, E. A. & Vining, G. G. 2012. *Introduction to linear regression analysis*, John Wiley & Sons.

Morris, C., Simmonds, I. & Plummer, N. 2001. Quantification of the influences of wind and cloud on the nocturnal urban heat island of a large city. *Journal of Applied Meteorology,* 40**,** 169-182.

Muller, C. L., Chapman, L., Grimmond, C., Young, D. T. & Cai, X. 2013. Sensors and the city: a review of urban meteorological networks. *International Journal of Climatology,* 33**,** 1585-1600.

Mutiibwa, D., Strachan, S. & Albright, T. 2015. Land surface temperature and surface air temperature in complex terrain. *IEEE Journal of Selected Topics in Applied Earth Observations and Remote Sensing,* 8**,** 4762-4774.

Nichol, J. & Wong, M. 2008. Spatial variability of air temperature and appropriate resolution for satellite‐derived air temperature estimation. *International Journal of Remote Sensing,* 29**,** 7213-7223.

Oke, T., Johnson, G., Steyn, D. & Watson, I. 1991. Simulation of surface urban heat islands under 'ideal'conditions at night Part 2: Diagnosis of causation. *Boundary-Layer Meteorology,* 56**,** 339-358.

Oke, T., Mills, G., Christen, A. & Voogt, J. 2017. *Urban Climates*, Cambridge University Press.

Oke, T. R. 1982. The energetic basis of the urban heat island. *Quarterly Journal of the Royal Meteorological Society,* 108**,** 1-24.

Oke, T. R. 1988. The urban energy balance. *Progress in Physical geography,* 12**,** 471-508.

Oke, T. R. 2002. *Boundary layer climates*, Routledge.

Peacock, J. 1983. Two-dimensional goodness-of-fit testing in astronomy. *Monthly Notices of the Royal Astronomical Society,* 202**,** 615-627.

Peng, S., Piao, S., Ciais, P., Friedlingstein, P., Ottle, C., BréOn, F. O.-M., Nan, H., Zhou, L. & Myneni, R. B. 2011. Surface urban heat island across 419 global big cities. *Environmental science & technology,* 46**,** 696-703.

Runnalls, K. & Oke, T. 2000. Dynamics and controls of the near-surface heat island of Vancouver, British Columbia. *Physical Geography,* 21**,** 283-304.

Shao, Y., Molnar, L. F., Jung, Y., Kussmann, J., Ochsenfeld, C., Brown, S. T., Gilbert, A. T., Slipchenko, L. V., Levchenko, S. V. & O'neill, D. P. 2006. Advances in methods and algorithms in a modern quantum chemistry program package. *Physical Chemistry Chemical Physics,* 8**,** 3172-3191.

Spruyt, V. 2014. *How to draw a covariance error ellipse* [Online]. Available: http://www.visiondummy.com/2014/04/draw-error-ellipse-representing-covariance-matrix/ [Accessed].

Stewart, I. D. 2011. *Redefining the urban heat island.* University of British Columbia.

Stewart, I. D. & Oke, T. R. 2012. Local climate zones for urban temperature studies. *Bulletin of the American Meteorological Society,* 93**,** 1879-1900.

Streutker, D. R. 2002. A remote sensing study of the urban heat island of Houston, Texas. *International Journal of Remote Sensing,* 23**,** 2595-2608.

Stull, R. B. 1988. Mean boundary layer characteristics. *An Introduction to Boundary Layer Meteorology.* Springer.

Sun, H., Chen, Y. & Zhan, W. 2015. Comparing surface-and canopy-layer urban heat islands over Beijing using MODIS data. *International Journal of Remote Sensing,* 36**,** 5448-5465.

Tomlinson, C. J., Chapman, L., Thornes, J. E. & Baker, C. 2011. Remote sensing land surface temperature for meteorology and climatology: A review. *Meteorological Applications,* 18**,** 296-306.

Van Hove, L., Jacobs, C., Heusinkveld, B., Elbers, J., Van Driel, B. & Holtslag, A. 2015. Temporal and spatial variability of urban heat island and thermal comfort within the Rotterdam agglomeration. *Building and Environment,* 83**,** 91-103.

Voogt, J. A. & Oke, T. 1998. Effects of urban surface geometry on remotely-sensed surface temperature. *International Journal of Remote Sensing,* 19**,** 895-920.

Voogt, J. A. & Oke, T. R. 2003. Thermal remote sensing of urban climates. *Remote Sensing of Environment,* 86**,** 370-384.

Wan, Z. 2006. MODIS land surface temperature products users' guide. *Institute for Computational Earth System Science, University of California, Santa Barbara, CA*.

Wan, Z. 2007. Collection-5 MODIS land surface temperature products users' guide. *ICESS, University of California, Santa Barbara*.

Wan, Z. 2008. New refinements and validation of the MODIS land-surface temperature/emissivity products. *Remote sensing of Environment,* 112**,** 59-74.

Wan, Z., Zhang, Y., Zhang, Q. & Li, Z.-L. 2004. Quality assessment and validation of the MODIS global land surface temperature. *International journal of remote sensing,* 25**,** 261-274.

Warren, E. L., Young, D. T., Chapman, L., Muller, C., Grimmond, C. & Cai, X.-M. 2016. The Birmingham Urban Climate Laboratory—A high density, urban meteorological dataset, from 2012–2014. *Scientific data,* 3**,** 160038.

Wicki, A., Parlow, E. & Feigenwinter, C. 2018. Evaluation and modeling of urban heat island intensity in Basel, Switzerland. *Climate,* 6**,** 55.

Wilmers, F. 1990. Effects of vegetation on urban climate and buildings. *Energy and Buildings,* 15**,** 507-514.

Wilson, E. B. & Hilferty, M. M. 1931. The distribution of chi-square. *Proceedings of the National Academy of Sciences,* 17**,** 684-688.

Zhou, B., Lauwaet, D., Hooyberghs, H., De Ridder, K., Kropp, J. P. & Rybski, D. 2016. Assessing seasonality in the surface urban heat island of London. *Journal of Applied Meteorology and Climatology,* 55**,** 493-505.

Zibognon, M., Crago, R. & Suleiman, A. 2002. Conversion of radiometric to aerodynamic surface temperature with an anisothermal canopy model. *Water Resources Research,* 38.

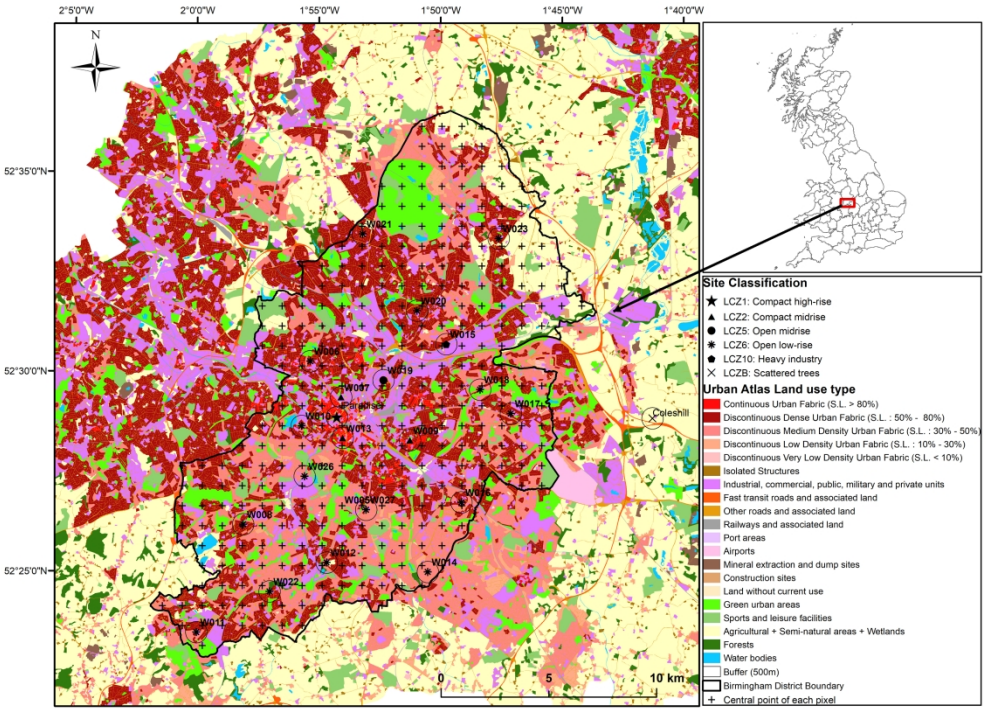

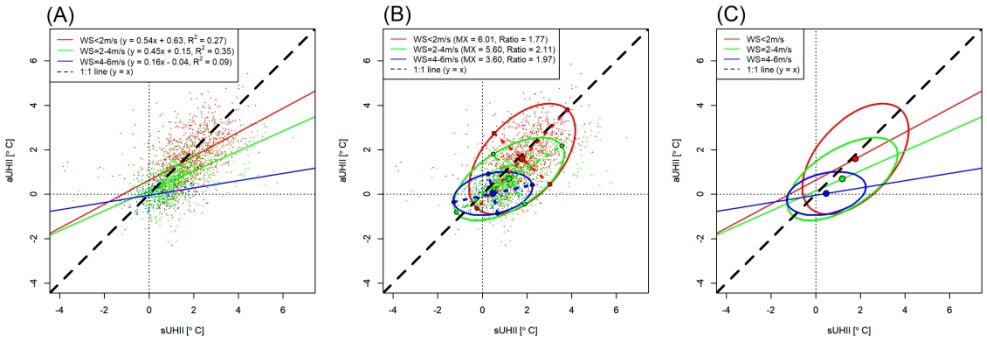

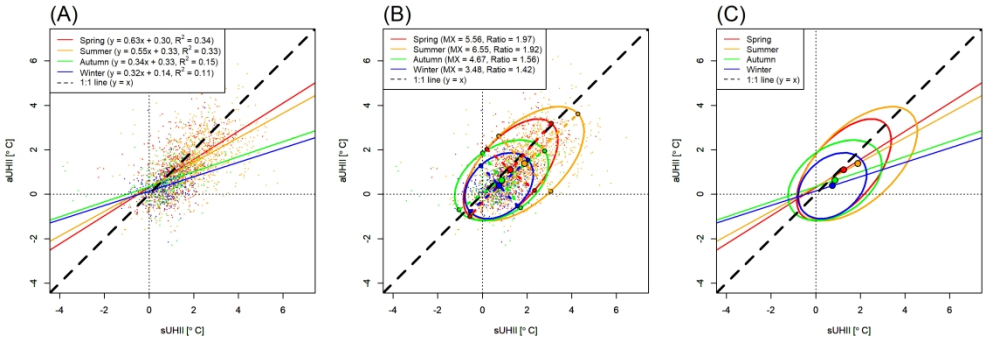

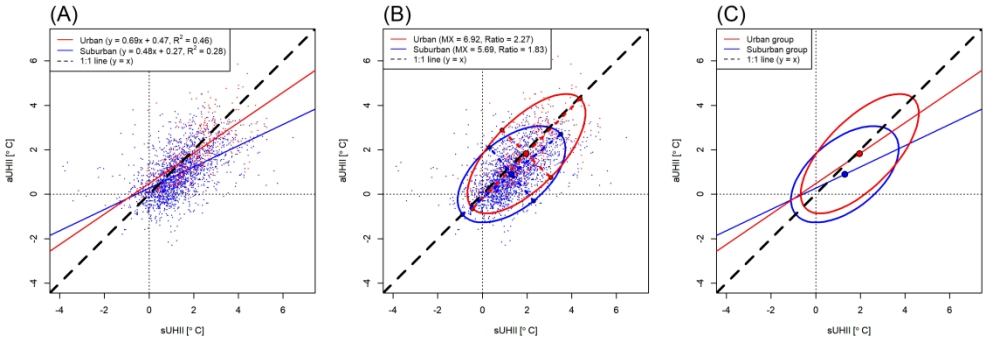

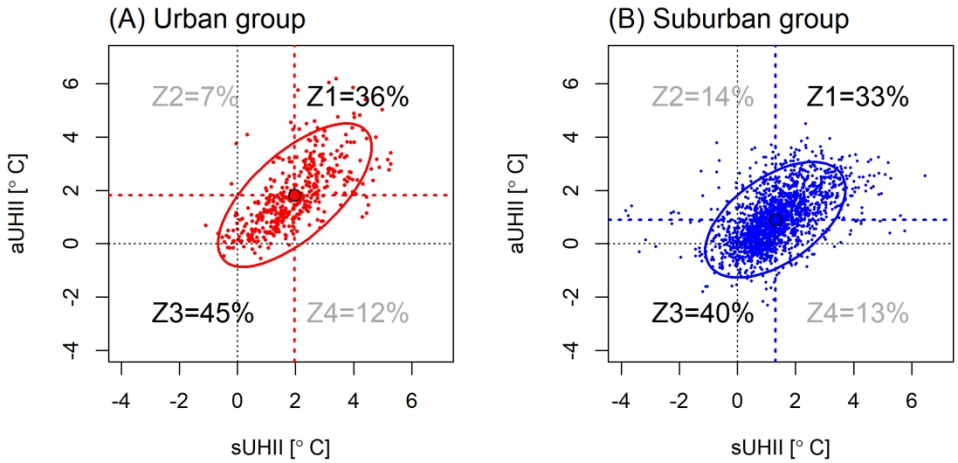

Table 1. Summary of previous studies on the T_s-T_a relationship in urban areas. NB: AGL, above ground level.

Study	Study area and period	T_s and T_a Data	Additional considered parameters	Temperature range (at night-time)	Derived R^2 (Nighttime)	Key findings
(Bahi et al., 2016)	Casablanca, Morocco; 2011-2012	T_s: MODIS Terra (MOD11A1) T_a: 9 weather stations (2 m AGL)	Day length, seasons, day/night	Not available	T_s~$T_{a(min)}$:0.92 T_s~$T_{a(max)}$:0.83	(a) Significant T_s-T_a correlation at nighttime; (b) Stronger relationship by separating data in summer and winter
(Azevedo et al., 2016)	Birmingham, UK; Summer (June, July, August), 2013	T_s: MODIS Aqua (MYD11A1) T_a: BUCL: 82 air temperature sensors and 25 automatic weather stations (3 m AGL)	Day/night, land use types	T_a: 11℃ ~ 14℃ T_s : 8℃ ~ 12℃ $\Delta T_{s-a}^{(i)}$: − 0.7℃ ~ 3.2℃	T_s~T_a: 0.6 T_s~T_a :0.8 ~ 0.99 ($single\ station$)	(a) Strong relationships in both day and night at neighbourhood scale but negligible relationship at city scale; (b) Stronger relationship at nighttime; (c) T_s and T_a are more dependent on land surface characteristics and advection, respectively
(Tomlinson et al., 2012)	Birmingham, UK; Summer (June, July, August), 2010	T_s: MODIS Aqua (MYD11A1) T_a: 28 sites with two iButtons for each site	Land cover data from MODIS	T_a: 12℃ ~ 22℃ T_s : 9℃ ~ 12℃ $\Delta T_{s-a}^{(i)}$: 1.67℃ ~ 6.39℃	T_s~T_a :0.51 ~ 0.95 ($single\ station$)	(a) No clear relationship at city scale; (b) Strong relationship at neighbourhood scale and the relationship varied between each station

Table 2. Summary of the available satellite imageries and sample size according to different moderate variables. NB: total sample size from all stations is based on the availability of T_s and T_a for each station.

Moderate variable	Group	Available imagery for Aqua satellite	Available imagery for Terra satellite	Total sample size from all stations (combined two satellites)
WS	WG1: 0-2 m/s	33	39	1073
	WG2: 2-4 m/s	27	45	1127
	WG3: 4-6 m/s	3	4	116
Season	Spring	14	21	660
	Summer	29	46	1048
	Autumn	10	13	351
	Winter	10	8	257
Site classification	Urban group	63	88	432
	Suburban group	63	88	1884

*Table 3. ANCOVA results based on the updated wind speed groups, where " ≠ " means "reject null hypothesis" — significant different (slope and intercept) or significant interaction effect exists (WS effect) (0.001***, 0.01**, 0.05*, 0.1)*

Base level	Slope	Intercept	Interaction effect
WG1 (WG2, WG3)	WG1≠WG2***, WG1≠WG3***	WG1≠WG2***, WG1≠WG3***	≠*** (F=9.77, p<0.001)
WG2 (WG3)	WG2≠ WG3**	WG2≠ WG3***	≠*** (F=12.81, p<0.001)

Table 4. D statistics from K-S test results based on the three wind speed groups where the significant tests reached 0.001 confidence level for all paired groups and the numbers in brackets are the $D_{\alpha(\alpha = 0.001)}$

Paired group	WG1	WG2	WG3
WG1	--		
WG2	0.39 (0.08)	--	
WG3	0.76 (0.19)	0.46 (0.19)	--

*Table 5. ANCOVA results (green highlight – interaction effect, blue highlight – significant tests of slope and intercept) based on the four seasons, where " = " means "cannot reject null hypothesis", " ≠ " means "reject null hypothesis" — significant interaction effect exists (seasonal effect) (0.001***, 0.01**, 0.05*, 0.1)*

Paired group	Spring	Summer	Autumn	Winter	Four seasons
Spring	--	(≠*, =)	(≠***, =)	(≠***, =)	--
Summer	≠* (F=3.44)	--	(≠***, =)	(≠***, ≠**)	--
Autumn	≠*** (F=27.45)	≠*** (F=14.61)	--	(=, ≠**)	--
Winter	≠*** (F=15.74)	≠** (F=7.35)	= (F=0.04)	--	--
Four seasons	--	--	--	--	≠*** (F=10.80)

Table 6. D statistics from K-S test results based on the four seasons where the significant tests reached 0.001 confidence level for all paired groups and the numbers in brackets are the $D_{\alpha(\alpha = 0.001)}$

Paired group	Spring	Summer	Autumn	Winter
Spring	--			
Summer	0.29 (0.10)	--		
Autumn	0.25 (0.13)	0.45 (0.12)	--	
Winter	0.43 (0.14)	0.55 (0.14)	0.22 (0.16)	--

*Table 7. ANCOVA results based on different LCZs and levels of urbanisation (green highlight – interaction effect, blue highlight – significant tests of slope and intercept), where " = " means "cannot reject null hypothesis", " ≠ " means "reject null hypothesis" — significant interaction effect exists (0.001***, 0.01**, 0.05*, 0.1)*

Paired group	LCZ1	LCZ2	LCZ5	LCZ6	LCZ10	Urban group	Suburban group	All LCZ
LCZ1	--	(=, ≠***)	(≠***, =)	(=, ≠**)	(≠***,≠***)	--	--	--
LCZ2	= (F=0.66)	--	(≠***, =)	(=, =)	(≠***, =)	--	--	--
LCZ5	≠** (F=9.99)	≠*** (F=10.87)	--	(≠**, =)	(≠*,≠**)	--	--	--
LCZ6	= (F<0.01)	= (F=0.14)	≠** (F=10.22)	--	(≠, =)	--	--	--
LCZ10	≠** (F=7.87)	≠*** (F=11.10)	≠* (F=3.24)	≠* (F=2.90)	--	--	--	--
Urban group	--	--	--	--	--	--	(≠***,≠***)	--
Suburban group	--	--	--	--	--	≠*** (F=11.20)	--	--
All LCZ	--	--	--	--	--	--	--	≠*** (F=8.979)

Table 8. D statistics from K-S test results for different LCZs where the significant tests reached 0.001 confidence level for all paired groups and the numbers in brackets are the $D_{\alpha(\alpha = 0.001)}$

Paired group		LCZ1	LCZ2	LCZ5	LCZ6	LCZ10
		Urban group		Suburban group		
LCZ1	Urban group	--		0.32 (0.10)		
LCZ2		0.24 (0.20)	--			
LCZ5	Suburban group	0.36 (0.26)	0.23 (0.23)	--		
LCZ6		0.44 (0.17)	0.32 (0.12)	0.33 (0.21)	--	
LCZ10		0.42 (0.27)	0.28 (0.24)	0.34 (0.29)	0.27 (0.21)	--

Table 9. Statistical quantities related to $sUHII$ and $aUHII$ *for different wind speed groups, season groups and urban/suburban groups.*

Moderate variable		$Cov(sUHII, aUHII)$	SD_{sUHII}	SD_{aUHII}	SD Ratio ($=\frac{SD_{aUHII}}{SD_{sUHII}}$)	Slope from LRM
WS	WG1	0.66	1.11	1.16	1.05	0.54
	WG2	0.59	1.15	0.87	0.76	0.45
	WG3	0.11	0.81	0.45	0.56	0.16
Season	Spring	0.61	0.99	1.07	1.08	0.63
	Summer	0.85	1.24	1.19	0.96	0.55
	Autumn	0.32	0.96	0.84	0.88	0.34
	Winter	0.16	0.71	0.69	0.97	0.32
Site characteristic	Urban group	1.04	1.23	1.25	1.02	0.69
	Suburban group	0.60	1.12	1.01	0.90	0.48